IRACST – International Journal of Computer Networks and Wireless Communications (IJCNWC), ISSN: 2250-3501
Vol.11, No 1, Jan– Mar 2021

Ground effect aerodynamics research that combines computational and experimental fluid dynamics.

T J Barber*, G Doig, C Beves, I Watson, and S Diasinos
School of Mechanical and Manufacturing Engineering, University of New South Wales, Sydney, Australia

Abstract: In this piece, we focus on the'synergistic' use of experimental and computational fluid dynamics (EFD and CFD, respectively), whereby the same researcher runs both sets of simulations simultaneously. In particular, case studies from ground effect aero- dynamics are presented, in which CFD and EFD were applied in the design of the primary facility. We next detail three case studies to illustrate the value of combining CFD and EFD analyses and the insights they provide. The analysis of a Formula-style front wing and wheel, the investigation of compressible flow ground impact aerodynamics, and the investigation of dimple flow (to improve aerodynamic performance) are the case studies. CFD has been used to not just supplement an experimental investigation, but also design the studies itself in several cases. It was found that laser-based, non-intrusive experimental procedures made for a great supplement to CFD. A novel post-processing approach has been devised, using the kriging and co-kriging estima- tors, to build correlations between the frequently dissimilar data types seen in the massive datasets discovered through experimental and numerical simulations.

INTRODUCTION

Simulating ground-effect aerodynamics Both CFD and EFD (experimental fluid dynamics) are often employed in the aerodynamics discipline. It is more typical, however, for the studies to be done independently by two different groups of researchers and then compared after the fact using two distinct datasets. In many cases, crucial (to the CFD practitioner) information is lacking, making it challenging to numerically duplicate the experimental circumstances. Although error analysis and comparison might be tedious, CFD can often be made to more accurately represent physical phenomena by simplifying the experiment.
therefore, it's no longer a valid basis for evaluating the trial results. The ideal situation would be for computations and experiments to be con- ducted in a "synergistic" fashion, where each approach informs the other, and where the final product of the research is enhanced because of t he collaboration between the two methods. This article provides case examples of synergistic research that combines CFD and EFD to better understand ground-effect aerodynamics. Each scenario involves the same investigator doing both computational and experimental experiments, with data from one kind of analysis informing the other (Fig. 1).
At UNSW, ground effect aerodynamics has been a hotspot for scholarship over the last decade. Some related factors have been discussed in our group.

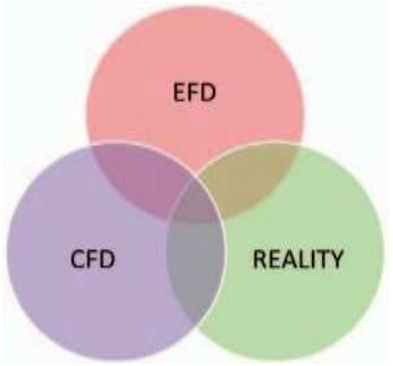

Fig. 1 Synergistic integration of CFD and EFD

fascinating domain of aerodynamics, and in every instance, CFD and EFD have been heavily used, in a fully integrated fashion. In many cases, this has been done because researchers want to examine a larger, more realistic version of the problem at hand. For example, while it is impossible to study a full-size Formula One car, good measurements can be made for a much smaller experimental case, and CFD can be performed for either case. More realistic results may be achieved by the combined use of CFD and EFD by integrating the findings and designing the overall approach for acquiring the flow field information. Our researchers are not restricted to a single field of expertise; instead, they must be well-versed in both CFD and EFD. Moreover, our team has been actively studying how to combine the two methods [2-4]. Only by combining them can the full benefits of integration be realized; for instance, tests will be planned with the CFD model in mind. Changing the proposed experiments somewhat may help with setting a more suitable limited CFD boundary condition.
To accurately experiment with ground effect for low ground clearances, such as those used in the automo- tive industry, a moving ground facility is required. Using computational fluid dynamics (CFD) examples of the many alternative ground plane representation techniques, we see that the flow field around the aerofoil is significantly altered by switching to an alternate approach [5].
Although subsonic applications have been the primary focus of ground effect aerodynamics research [6, 7],

transonic and supersonic applications in which ground proximity is an important parameter do exist, such as land speed record cars, low-flying military aircraft, or projectiles close to the ground or solid obstacles. Supersonic ground-effect aerodynamics investigations need careful consideration of the following factors:

presentation of the ground. While a moving ground would provide the best physical realism in a wind tunnel setting with a stationary model [6, 7], it is not feasible at supersonic speeds. Moving the object through still air using a rocket-sled testing facility [8] or a ballistic range [9] may seem like the simpler option, but this method comes with a number of drawbacks, including the increased complexity of all diagnostics related to free-flight measurements, high costs, and possible restrictions on access by the military.
In contrast, supersonic blowdown tunnels are rather widespread and easily accessible; this article describes a research that looked into whether or not the best methods for simulating ground effects at lower speeds might be used at higher speeds for supersonic applications in blowdown tunnels. A look is next taken at the transonic case study. Since generating a dynamic ground in CFD is so simple, numerical modeling played a crucial role in this procedure (Fig. 2). Two experimental alternatives that were less desirable than the ideal one were then evaluated.
CFD was utilized in the preliminary phases of the design of the transonic trials, first to establish circumstances at which early commencement of shock waves was expected owing to the ground effect, and then to modify the design of the sting and endplates to cause little interference to the flow on the wing (s). This numerical software found that the tunnel walls and endplates would still have a significant impact on the flow. Two-dimensional (2D) (2D)

Fig. 2 Role of transonic experiments in cooperation with CFD

The experimental program's computational fluid dynamics (CFD) analysis confirmed the need for a comprehensive three-dimensional (3D) representation of the equipment. It was only by comparing the high-fidelity numerical findings to the wind tunnel data that we were able to learn about aspects of the flow-field, such as transient shock movement and boundary layer behavior, that couldn't have been identified from the experiments alone.

an overview of experimental and computational methods

Subsonic experimental measurements were taken in a 235 x 340 mm2 UNSW moving ground wind tunnel (see Fig. 3). Screens designed to reduce turbulence are placed between the intake fairing and the 7.8:1 contraction ratio portion, and a 5-Hp fan is utilized to push the air down the tunnel. The laser doppler anemometry (LDA) recorded free stream flow angularity was less than 0.2o and indicative of a well-mixed test section flow.

The highest speed of the test segment is 15 m/s, and the turbulence severity is 1%.
The utilization of non-intrusive measurement methods that generated copious quantities of field data (for better comparison with numerical findings) was a top priority throughout the design phase of this facility, which was intended for projects with a substantial CFD component. Throughout the tunnel, measurements are taken using three different major systems.
Use of several He-Ne and Nd-YAG lasers, smoke for seeding, and digital camera recording to create a qualitative flow field visualization.
Particle imaging velocimetry (PIV) quantitative analysis performed in-house. The main laser for the PIV system is generated by an EKSPLA NL301-2G unit, which consists of two lasers (each having a Nd:YAG rod, flash-lamp, and Pockels Cell) and a dichroic mirror to split the green wavelength (532 nm) from the red wavelength (660 nm).

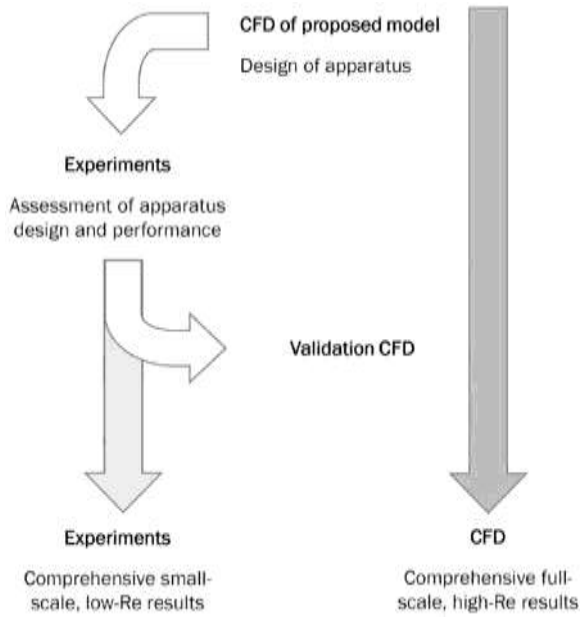

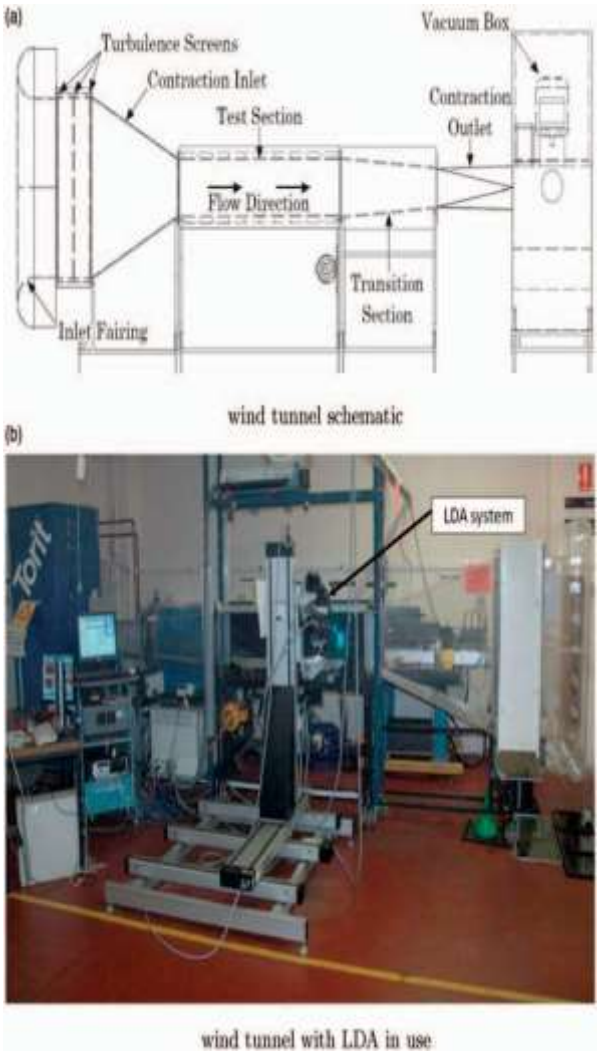

Fig. 3 225 x 340 mm^2 UNSW wind tunnel

infrared (1064 nm) (1064 nm). VidPIVv4.6 from ILA GmbH, a commercially available image analysis program, may be used to process the collected pictures.

Analyses performed quantitatively using a Dantec 3D LDA system. The main beam is supplied to the transmitter box from a Coherent INNOVA 70C 5W Argon Ion (Arg-Ion) laser, and from there it is distributed to the LDA probe heads. The lightweight three-axis traverse system supports the 85 mm probe heads, which operate in a 3D coincident backscatter mode. The high throughput was made possible by a novel alignment method that made use of a CCD camera to align the beam to a resolution of only 5 pixels.

To enable laser flow measurement methods to be employed anywhere in the tunnel, the tunnel walls (and many model components) were made from high grade perspex. If you use atomized vegetable oil for LDA or PIV, you'll receive particles with a diameter of 1 mm and a slip velocity of less than 1 percent.

To guarantee the wind tunnel built would provide the necessary flowfield, many CFD models were created before construction began. Using the use of a 3D model of the tunnel's intended environment, the optimal placement with respect to the walls was determined [10]. Several potential configurations of the tunnel's moving ground and the removal of the boundary layer at the tunnel's leading edge were simulated in a comprehensive 2D model. It was anticipated that the ground's motion would introduce turbulent energy into the flow, thus CFD was used to first design for the most consistent flow possible and the least amount of turbulence possible across the test segment. Two-dimensional finite-volume numerical methods were used for the calculations. Advanced wall treatment due to pressure gradients is possible in Reynolds-averaged Navier-Stokes (RANS) simulations using the k-e RNG turbulence model with a grid size of 350 000 points and wall y=142*. In the 340 x 225 mm2 cross-section test section, 10 m/s was the desired operational free stream velocity (ReH = 2.8 x 105). Numerical study and research into existing facilities [11, 12] informed the development of the intake for the contraction and the test section expansions. The tunnel and moving ground were built internally, and measurements were made using the LDA system to verify the flow-field in the test section after the design was finalized. The 2D probe used to conduct the LDA measurements was tilted downwards towards the belt so that the readings would be as near as possible to the belt's surface. Several locations throughout the test portion were used to collect velocity profiles;

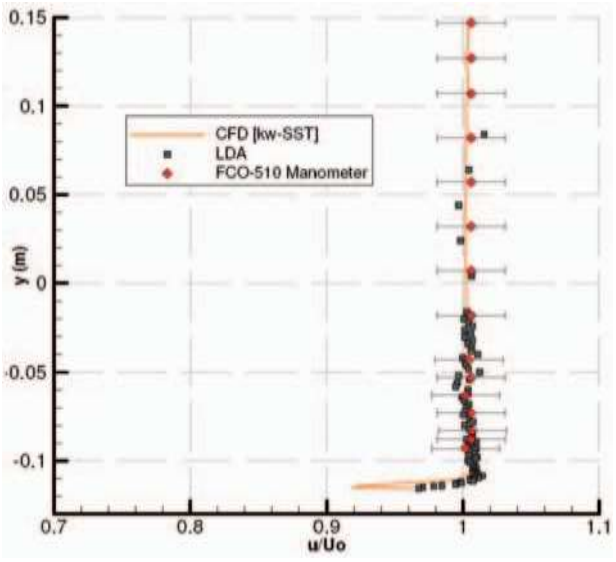

Fig. 4 Velocity profile in test section, and comparison with CFD results

Figure 4 depicts a common CFD comparison, which involves the evaluation of numerical forecasts against 2D LDA and Pitot-static data (where u is the local velocity and Uo is the freestream velocity). Although the CFD model predicted that the boundary layer would be fully eliminated at the ground, this did not happen in practice. Nonetheless, both the height and the change in velocity inside the boundary layer are small enough to be ignored.

In our lab, we often run CFD simulations with the help of the Fluent finite volume RANS solver (some research is carried out using LES but this is not detailed in this

article). Gambit, a mesh generator, is often used to create new meshes. The need of validation and verification is emphasized to adhere to the guidelines set out by Roache [13] and the AIAA [14]. Our in-house cluster is an SGI Altix 4700 64-bit shared memory system with 128 Dual-Core 1.6-GHz CPUs and 1 TB RAM, while our remote ac3 (ac3.edu.au) cluster is situated in Australia and runs Fluent on Linux.
By directly monitoring the velocity dis- tribution and turbulence intensity for the relevant test using the 3D LDA system, correct boundary conditions were attainable for comparisons with tests in the moving ground wind tunnel. The models used in the wind tunnel and the tests included full CAD data, therefore the numerical model's dimensions were accurate to within the typical manufacturing tolerance of 0.01 mm.

Summary

This article provides three concrete examples to illustrate the unified procedure of
using CFD and EFD:
aerodynamics of a formula-style racing car's wing and wheel; aerodynamics of high-velocity (compressible) flow ground effect conditions; the flowfield in a dimple, which might be utilised to improve aerodynamic performance.

When used in tandem, CFD and EFD may provide massive data sets for otherwise equivalent setups. Point velocities, temperatures, pressures, turbulent components, etc., are examples of spatially-located data that may be found dispersed over a computational domain or experimental area of interest. Both datasets include room for mistake and ambiguity, yet a comparison must be done nevertheless. In many cases, the initial data from the field is compared visually, point by point, and with a fair amount of qualitative judgment. It would be very helpful if there was a meaningful and quantifiable mechanism to compare, interpolate, and cross-correlate the various spatial data. In the article's closing paragraphs, the kriging estimator is presented as a potential method for combining the two datasets in a logical fashion. Now, the second case study (including the interaction between the wing and the wheel) is utilized to illustrate the utility of the newly created approach.

INDIVIDUAL CASES

Examples: dimples on wings

Embedded dimples on a flat surface have been shown to be effective in blending the boundary layer [15–17]. The dimple flow structure has been the subject of previous computational studies, with just a few flow visualization experiments available for comparison. The dimpleo shape and dimple-based Reynolds number utilized as references in various examinations by different researchers did not always match up, making it difficult to validate and verify the numerical model employed in these studies. In this investigation, the impact of dimples added to ground effect wings to improve aerodynamic performance was studied using the recently created tunnel without the moving ground facility. At first, the flow inside of a single dimple was investigated using LDA and PIV. The dimple had a depth of 8 14 19.8 mm and a print diam- eter of D 14 90 mm, for a dimple depth-to-diameter ratio ( ) of 8/D 140.22. Using the dimple print diameter as a proxy for the Reynolds number (ReD), we get 9.0 x 103 for the test section height H/D & 3.55. Researchers compared the dimple's velocity as measured in the lab to that seen in the real world.

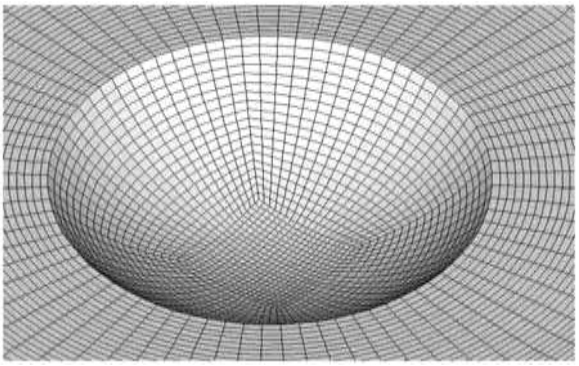

Fig. 5 Fully structured hexahedral mesh on the dimple surface

same wind tunnel shape, Reynolds number, and turbulence intensity are applied to a steady-state RANS CFD model. The dimple's grid is completely organized, using hexahedral pieces throughout the board (Fig. 5). After the numerical model had been verified, we could use the verified findings to learn more about the flow field.
In the laboratory, a dimple of the same size was used to replicate the results. The LDA probes were placed such that their beams would record three velocity components down to the surface of the dimple without being interrupted by the spanwise rim of the dimple. The results were impacted up to 2 mm from the surface, despite the fact that anodizing the surface matt black helped reduce light reflection off the aluminum.
PIV cross-correlation analysis is "smoother" than the LDA, which only collects point measurements, since it uses a grid of 64x64 pixels and a 12-pixel overlap to resolve the flow field. Using LDA, we were able to collect information from

The PIV camera was configured to take 1000 picture pairs in 1.5 s at an average data rate of 1500 Hz and a peak of 3500 Hz above the dimple, with a sample rate of 2000 samples (over 180 s). Only the streamwise and normal veloci- ties are measured since the PIV system is only 2D. By matching the intake boundary condition velocity and turbulence intensity with the experiment, the numerically projected boundary layer is more in line with the LDA observed boundary layer upstream of the dimple (Fig. 6).
The streamwise flow component is characterized by an

area of reversed flow under the dimple rim from y/D - 0.05, which decreases in size and strength as the distance from the leading edge of the dimple increases (Figs. 7 and 8).

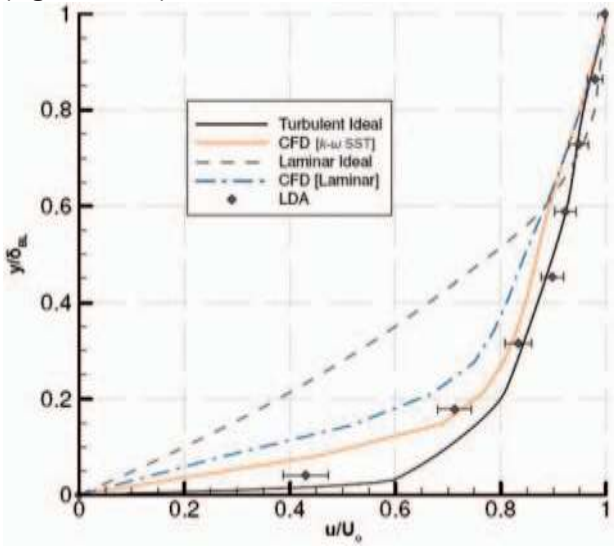

Fig. 6 Boundary layer profile 30 mm upstream of dimple, 8_{BL} & 24.3 mm

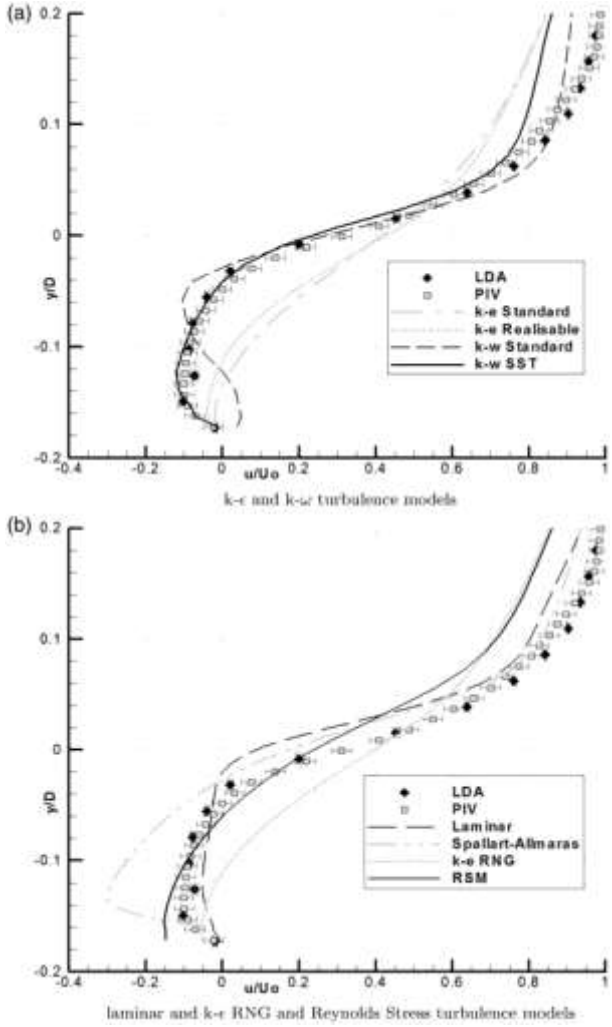

Fig. 7 Position 1 *u*/Uo turbulence model comparison Re_D ¼ 9.0 x 10^3

The crease deepens. Beyond the first shear layer separation from the dimple's leading edge is the recirculation area. When one approaches the dimple's downstream face, the shear layer at y/D & 0.05 begins to collapse. Comparing the LDA and PIV data with the k-e standard and k-c SST turbu- lence models, the latter two fare better.

The stream-wise velocity profiles predicted by the conventional, RNG, and realizable k-e turbulence models are comparable. The dominant aspect is the absence or very little amount of reversed flow in the LDA and PIV data; in fact, the streamwise flow component is reversed only at position one for y/ D - 0.125, but in the experimental data, it is reversed at all three places. Weak shear layer shown by almost linear u/Uo profile between locations 1 and 3. The k-e turbulence models largely under-predict the streamwise flow within the dimple, albeit there is some resemblance to the experimental flow profile.

At all three locations, the laminar model more accurately captures the general trend of the observed streamwise velocity profile than does the Spalart-Allmaras model. As compared to LDA and PIV data, the magnitude of the reversed flow is somewhat smaller, suggesting a larger-scale'stalled' flow zone just below the dimple rim. Although the laminar model predicts a larger'stalled' flow zone in line with the dimple rim (y/D 14 0) than the actual flow recirculation, which is located deeper under the rim of the dimple (y/D -0.05), the shear layer anticipated by this model is similarly located higher. Nevertheless, the initial recirculation in the upstream surface of the dimple predicts a significantly wider recirculation zone, with stronger reversed flow than found in the actual findings, suggesting the one equation Spalart-Allmaras turbulence model over-estimates the experimental data. Because of the increased recirculation of the flow, the shear layer is predicted to be located significantly higher than in experiments.

Below the dimple rim (y/D 0), the streamwise projected flow profiles for the Reynolds stress model inside the dimple show a decent degree of consistency. The shear layer and boundary layer streamwise flow is well predicted above the dimple rim, in contrast to the LDA and PIV findings, which exhibit poor agreement.

In an effort to provide an explanation for the outcomes seen in the experimental data, a visualization of the CFD flowfield was used (using the k–c SST turbulence model). Figure 9 displays the pathlines within the dimple, revealing two lateral vortex cells that sit just below the dimple's outer rim. At low Reynolds numbers, as seen in Fig. 9(a), two symmetric vortex cells are created, with their core fluid coming from the upstream half of either side of the dimple.

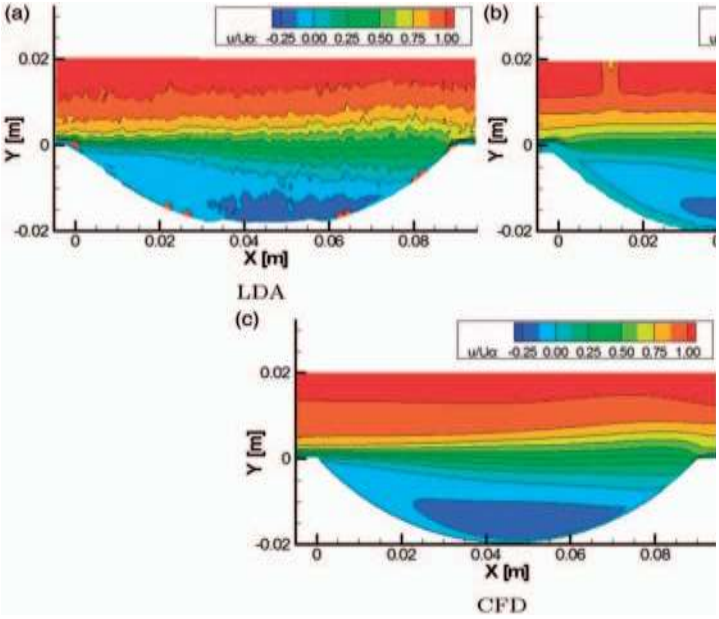

Fig. 8 Normalized streamwise velocity LDA Re_D ¼ 9.0 x 10^3

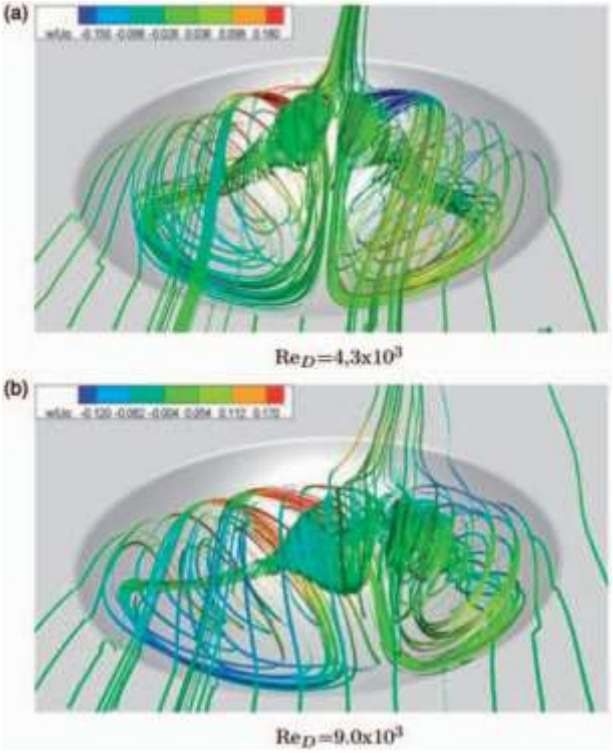

Fig. 9 3D flow field in the dimple

encompassing the whole area of the dimpled surface. Chew and Khoo [18] observed that when the Reynolds number is raised, the flow field in the dimple becomes asymmetric, with one vortex cell becoming dominant. This is shown in Figure 9(b). Also, the weaker organism's central fluid is clearly visible.

When the flow approaches the dimple, a vortex forms on the downstream half of the dimple's surface.

In Fig. 9, the pathlines are colored by w/ Uo, revealing the extent of the positive and negative spanwise flow zones as well as the peak positive and negative values. Since the spanwise velocity intensity (w) on the downstream face of the dimple is increased by the stronger vortex cell at the higher Reynolds number, fluid is now fed from the downstream face of the dimple into the weaker vortex area. When the Reynolds number increases, this hinders the development of the vortex in the right side of the dimple. With the help of the dimple's enlarged positive area of spanwise velocity, the primary vortex is able to grow in length.

The experimental study does not provide this level of detail about the flow field, but a careful comparison with the available experimental data provides confidence in the numerical conclusions and makes the 3D information clear.

Case study 2: wheel and wing

The aerodynamics of racing cars are often studied in isolation, with researchers examining things like inverted wings in ground effect [19], diffusers [20], cylinders [21], and exposed wheels [22-24]. In this research, we employed the mobile ground wind tunnel with an ancillary numerical analysis to investigate the front wing and wheel aerodynamics in Formula One style.

Two numerical models, one representing the wind tunnel and the other the full-scale racing vehicle condition, were created. The validation gap for full-scale circumstances was addressed by comparing wind tunnel findings with the corresponding CFD since experiments could not be undertaken (Fig. 10). The purpose of this full-scale computer model is to accurately simulate the environmental factors that affect the performance of a combined wing and wheel on a standard open-wheel racing vehicle. The Reynolds number was calculated using a model of a full-size NACA4412 wing and wheel (chord and diameter, respectively, of 562.5 and 660 mm).

1.28 x 106, determined from the span of the wings, and 1.50 x 106, calculated from the diameter of the wheels. Because of its widespread use in research on ground-effect aerodynamics, the NACA4412 profile was chosen for this analysis. The experimental setup was recreated in the scaled CFD model, with the mesh utilized shown in Fig. 11. Attempts were made to preserve as many of the full-size computational model's properties as feasible. When compared to wind tunnel models, the wing chord and wheel diameter are spot-on (75 and 88 mm, respectively, giving a scale of 1:7.5). Using the wing chord as the standard, the wind tunnel tests (and corresponding CFD simulations) were run at a Reynolds number of 5.11 x 106. (or 5.98 x 106 based on the wheel diameter). Not enough force was applied to the boundary layer to trigger it.

to promote transition in either the computational or

experimental simulations.

Fig. 11 Surface mesh indicating grid structure

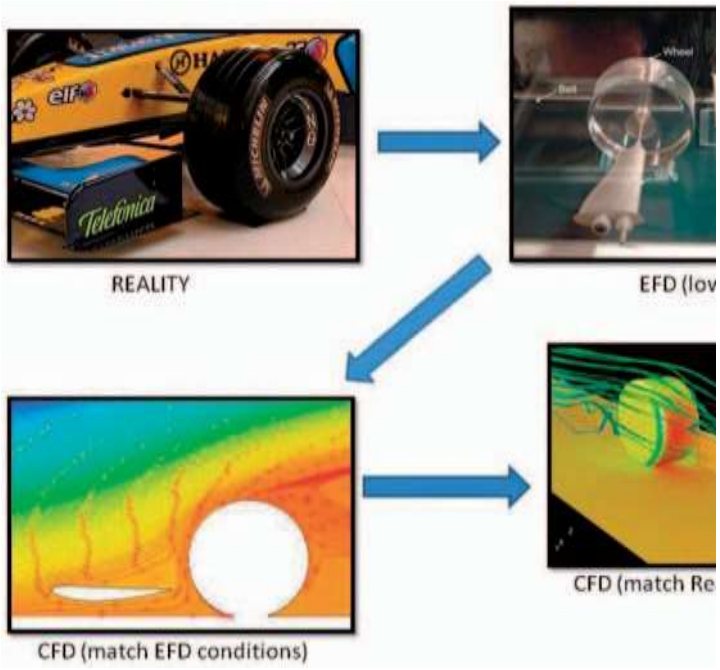

Results obtained with several different turbulence models were compared to LDA measurements made in the wake of the wing and the wheel in order to determine the most suitable turbulence model and to demonstrate that the computational model can accurately reproduce the variations in flow structures associated with changes in the wing span and angle of attack of the wing (parameters that were investigated in a further wing and wheel interaction study). An example is given in Fig. 12, showing the *x*-velocity on the $x/c = 0.75$ plane (just downstream from the wheel – see Fig. 19 later in this article for a further representation), where *c* is the wing chord.

to leverage numerically expensive information [32]. It is essentially a technique for spatial interpolation that fits a stationary random function to a set of sampled known point values, thus producing a response surface. The interpolates are weighted averages of the point values, and the weights are calculated in such a way as to minimize the modelled kriging variance of the estimate [33]. The kriging variance itself is representative of the modelled uncertainty of the estimate at some remote point, and it is dependent upon the statistical continuity of the data. Kriging has a number of advantages as an estimator. It is the best linear unbiased estimator (BLUE) and without a so- called nugget effect, it will construct a response sur- face that exactly interpolates the known data. Cokriging extends the basic interpolation capabilities of kriging to multiple correlated datasets.

Kriging can be viewed as a non-parametric interpolator – it fits a response surface through a given set of known data points by assigning weights to the data. However, unlike other common non-parametric

Fig. 10 Description of methodology

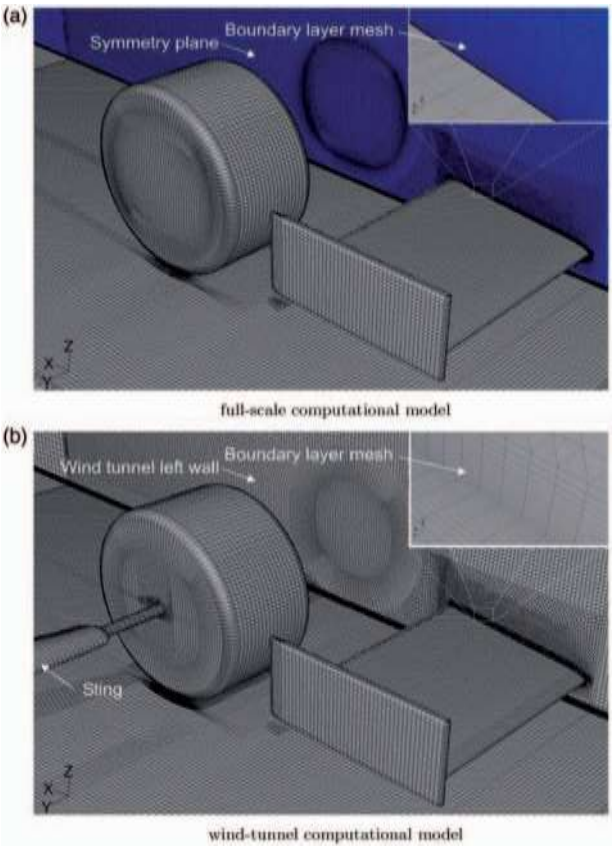

interpolation methods, its basis functions derive from an underlying statistical model. An attempt is made to characterize the smoothness (spatial conti- nuity) of the complete phenomena based on such nodal data as are available for interpolation and to this end, covariance functions of the data are esti- mated, so that a model for spatial continuity may be determined. There are two steps for estimation. The first is structure identification, which informs the the- oretical random function model, and the second is estimation, in which this model is used to form a covariance matrix which may be solved for the linear weights. A particular random function is notated P^P. A random function P^P is characterized by its covariance function; $C_{PP}(x, y)$. This expresses the covariance between the regionalized random var- iables $P^P(x)$ and $P^P(y)$, which measures the strength of the relationship between data located at *x* and data located at *y*. In the context of estimation, this provides a means of gauging the relative importance of the surrounding data, and is appropriate where data is spatially dependent. Fundamentally, it is assumed that the spatial data for interpolation are a realization of a given random function – a regionalized random variable. If there are secondary data that are expected to be strongly correlated to the primary variable, it should be possible to improve the estimate by its consideration. In this case, the concepts are extended by

Here, the developed kriging algorithm has been applied to the wing and wheel study discussed earlier (section 2.2). The velocity components are consid- ered as independent, Gaussian, realizations of a random function with an unknown drift. The

Structure identification follows the steps outlined in the 'Model for covariance' section, and drift estimates are calculated using Universal Kriging methods. Using nodal values, kriging creates an interpolated response surface as its principal output.

Con- tours of x-velocity are presented in Fig. 20 with experimental (LDA) findings on the left and CFD results on the right, representing the original data. The measuring grid is also shown in the LDA photos. Figure 19 displays the findings over five separate measurement planes, each represented by one of the five photos.

Based on the strong spatial correlation between the cokriged data (Fig. 21), it is evident that the wake behind the wheel may be included into the experimental result. Also, the boundary layer at the moving ground beneath the stagnation zone in front of the wheel is made more obvious, and the interaction with the moving ground below the wing is edited in.

The third-slice cokriging is similarly affected by the new information, but less noticeably. The LDA's coarse sampling makes it difficult to determine the structure of the little wake behind the sting outboard (to the right) of the wheel wake, but doing so with the numerical result makes the structure more clear.

Figure 20 shows how the area in front of the wheel wake is also sampled roughly, leading to many altered structures in the cokriged estimations shown in Figure 21. The whirlpool

Additional numerical data provides a good description of the amplification in the region inboard of the wing. When the bottom of Fig. 21 approaches the shifting ground, a strong bound- ary layer forms. Nonetheless, numerical data must resolve the boundary layer, either by wall functions or local mesh refinement, even when experimental data are rather sparse (and in any case incorrect) near the walls and limits of the wind tunnel. Combining these two extremes is what cokriging does.

The third slice also shows a change to the low x-velocity zone just behind the wheel, where the complex vortex structure indicated by the computational calculations is now hardly perceptible.

There is still a lot of effort to be done in order to develop a closed-form post-processing tool by expanding the capabilities of existing algorithms to handle bigger and more demanding tasks. It has been shown, however, that the suggested methods may be used to provide a more accurate image of the overall findings correlation and present the 'best' overall estimations of crucial factors.

CONCLUSIONS

The effective and synergistic combination of CFD and EFD has been shown using examples drawn from ground effect aerodynamics research. Most of the work is carried out experimentally in a moving ground wind tunnel, the creation of which is an example of the combined use of CFD and EFD to get the desired result. The use of non-invasive measuring methods has the added benefit of generating copious volumes of useful

Fig. 20 : Raw x-velocity for LDA and CFD

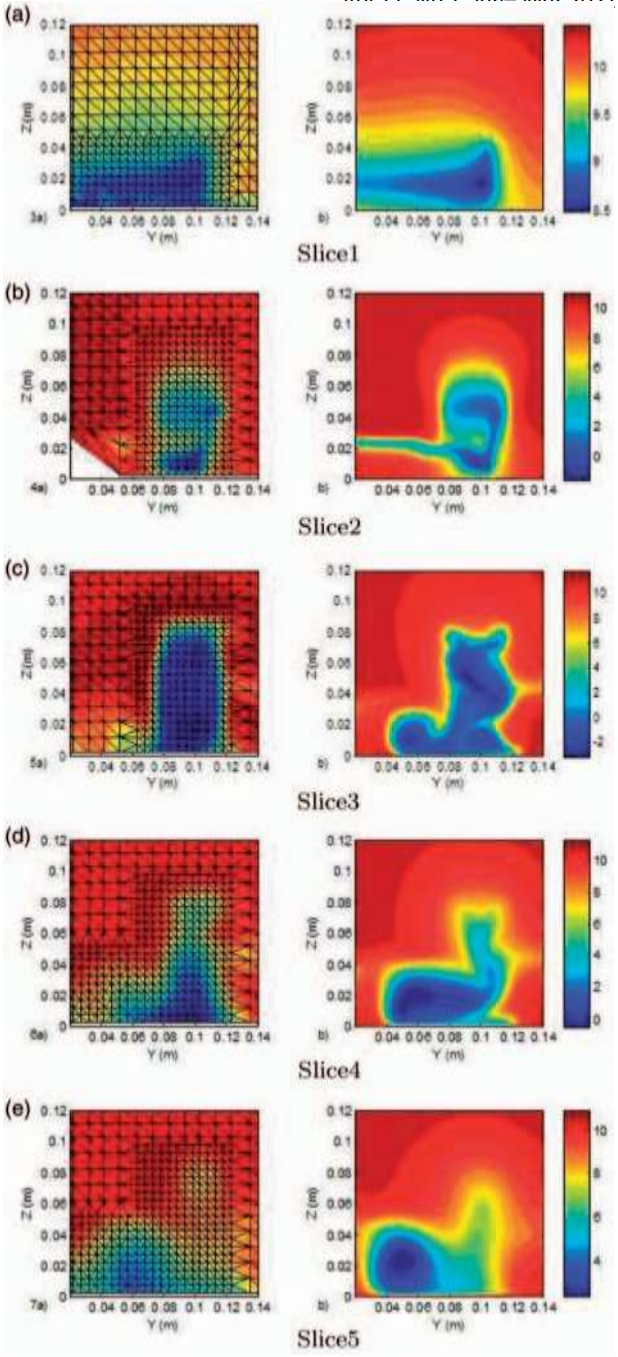

field data (for better comparison with CFD results).

The movement of fluid within of a single dimple was investigated. This was an exploratory work that opened the door for more thorough examination of how dimples can improve the aerodynamic efficiency of ground-effect wings. Using the same wind tunnel dimensions, Reynolds number, and turbulence intensity, the steady-state CFD model was compared to the experimentally recorded velocity in the dimple. The experimental data was used to confirm the numerical model, and the verified findings provided insight into the flow-field that had been previously unavailable. In this case, the experimental data revealed a specific flow behavior, which was then studied numerically.

Two computational fluid dynamics (CFD) models were created to investigate the aerodynamic interaction between a Formula One-style front wing and wheel.

In a wind-tunnel. As full-scale tests could not be performed, the validation gap was closed by comparing wind tunnel data with the matching CFD. In order to determine the most appropriate turbulence model and to demonstrate that the computational model can accurately reproduce the variations in flow structures associated with changes in wing span and angle of attack, results obtained with a number of different turbulence models were compared to LDA measurements made in the wake of the wing and the wheel (parameters that were investigated in a fur- ther wing and wheel interaction study).

The third instance included research into ground effect aerodynamics at both the supersonic and transonic speeds, and so required the utilization of a distinct facility. While the generation of a relocating ground is an easy procedure in CFD but not so empirically, this approach relied heavily on CFD modeling. The raised ground plane, which minimizes the bound- ary layer's size, and a symmetry ground condition, which calls for two identical models in the experimental situation, were both examined as potential ground simulation approaches. Supersonic and transonic instances were tested in a wind tunnel and compared to computer simulations of the wind tunnel conditions and a theoretical moving ground scenario. After discovering significant 3D effects throughout the experimental program, further numerical models were executed as complete 3D instances.

Ultimately, it is becoming more important to have a tool that can intelligently analyze all the data acquired via the various computational and experimental methods. With the use of the kriging estimator, it was proven in this research that two datasets may be combined in order to enhance each other, rather than only compared.

Each instance shown here is an example of a synergistic CFD and EFD study in which the same researcher conducted both the computational and experimental parts of the investigation. To reduce the possibility of researcher bias and validation mistakes (for instance, an error in utilizing erroneous geometry might be followed through in both CFD and EFD studies), it is important to compare your findings to those of other researchers' that have been published in credible journals.

FUNDING

There was no particular grant for this study from any government, business, or nonprofit organization.

REFERENCES

R. M. Cummings and K. Knowles. A guest column. Proceedings of the Institution of Mechanical Engineers, Volume 223: Issues 1 and 2, Journal of Aerospace Engineering, 2009.

Myre, D., Neely, A., Doig, G., and Barber, T. The use of experiments to verify computational fluid dynamics results is essential to the field. 2010;51(C2):C265–C279 ANZIAM J.

Barber, T.; Doig, G; Beves, C; Watson, I; and Diasinos, S. The merger of computational fluid dynamics (CFD) and experimental fluid dynamics (EFD) for research into ground effect aerodynamics was the topic of the keynote address. The von Karman Institute for Fluid Dynamics hosted a symposium on integrating computational fluid dynamics (CFD) with experimental work in aerodynamics on September 14-16, 2009 in Brussels, Belgium.

Aerodynamic ground effect: a case study of the combination of computational fluid dynamics (CFD) and experiments. Barber, T. J. Vehicle Design International, 2006, 40(4):299-316.

T. Barber, A technical comment on the proper CFD boundary conditions for the prediction of ground effect aerodynamics. Published in 1999 in Aeronautical Journal.

Theodore Barber; Elizabeth Leonardi; Robert Archer. Reasons for differences in ground-level impact studies. NASA Aeronautical Journal, 2002, 106(1066), pp.

The authors are B. Fago, H. Lindner, and O. Mahrenholtz. how ground-based wind-tunnel simulation influences vehicle-surrounding airflow. Aerodyn., 1991, 38, 47-57 in J. Wind Eng. Ind.

Rocket sled excitation for rail resonance: critical velocities. Lamb, J. Reference: Johns Hopkins APL Technical Digest, Volume 21 Issue 3 (2001), Pages 448-458.

John Purdon, Natalie Mudford, and Herbert Kleine. Projectiles traveling at high speeds near solid objects. Volume 6279, page 627929, 2007 Proceedings of the 27th International Conference on High-Speed Photography and Photonics, Society for Photographic Education (SPIE), Bellingham.

S. Diasinos; T. J. Barber; E. Leonardi; and S. D. Hall. Implementing a Moving Ground in a UNSW Wind Tunnel: Validation of a 2D Computational Fluid Dynamics Model. Paper 3.2 of the CD-ROM published proceedings of the 2005 Pacific Symposium on Flow visualization and image processing (PSFVIP5), Daydream Island, Australia, September 27-29, 2005.

The authors' full names are Barlow, J. B., Rae, W. H., and Pope, A. Studying the effects of low speeds in a wind tunnel: third edition (1998) (John Wiley and Sons, New York).

B. C. Motson and R. D. Archer. Wind tunnel design considerations for low-velocity applications, report no. 19969/FMT/3, 1969 (University of New South Wales, Australia).

Verification and validation in computing science and engineering. 1998, P. Roache (Hermosa, Alb- querque, Mexico).

The Aeronautics and Space Administration Professional Association of the United States.

Verification and validation procedures for computational fluid dynamics models. G-077- 1998, American Institute of Aeronautics and Astronautics.

Isaev, S., & Leont'ev, A. I., "Viscosity Effect on Vortex Dynamics in Laminar Separated Flow Past an Asymmetric Dimple on a Plane: Analytical Results," Physical Review E, vol. Engineering Physics and Thermophysics, 2001, 74 (2).

Authors: Mahmood, G., and Sabbagh, M. Z. Dimples and projections on opposing walls of a channel aid heat transmission. Journal of Thermophysics and Heat Transport, 2001, 15(3):275–283.

Nusselt number behavior on deep dimpled surface in a channel. Burgess, N., and Olivera, M. M. 2003, 125, 11-18 in J. Heat Transfer.

Flow visualization studies on flow structures inside of spherical dimples of varying depths and with/without

rounded edges. Chew, Y., and Khoo, B. C. Presented at the 5th PSFVIP, Melbourne, Australia, September 27-29, 2005. Proceedings, PSFVIP-5-280.

Ground-effect aerodynamics for a single-element wing. J. Zerihan and J. Zhang. 2000, J. Aircraft, 37(6), pp.1058-1064.

Experimentally determined optimal geometries for rectangular, canonical, and circular rectilinear diffusers. Sovran, G., and Klomp, E. D. Pages 270-319 of 1967's Fluids: The Mechanics of Internal Flows (Elsevier Publishing Co., New York).

The authors are S. Mittal and B. Kumar. Go around a revolving cylinder. 2003, 476, 303–334; J. Fluid Mech.

The aerodynamics of a single tire touching the ground, Fackrell, J. E. London University, Department of Engineering, Doctoral Dissertation, 1974.

We thank John E. Fackrell and John K. Harvey for their contributions to this article. The effects of wind on a single moving road wheel. This article may be found in the AIAA volume "Proceedings of the Second Symposium on Aerodynamics of Sports and Competition Automobiles," which took place in 1975 in Los Angeles, California (Western Periodicals Co., North Hollywood, California).

Aerodynamic features of automotive wheels: computational fluid dynamics (CFD) prediction and wind tunnel experiment. Axon, L. In terms of aerodynamics,

prediction using Computational Fluid Dynamics and wind tunnel testing on vehicle wheel designs.

In S. Diasinos et al. The dynamic interplay between a spinning wheel and a downforce-generating wing in ground effect. Dissertation for the degree of Doctor of Philosophy, University of New South Wales, 2009.

G. Doig, T. J. Barber, E. Leonardi, A. J. Neely, and H. Kleine. Strategy for studying the effects of the supersonic ground swell in a blowdown wind tunnel. (2008), Shock Waves, 18(2), 155-159.

Authors: Doig, G.; Barber, T.; Leonardi, E.; Neely, A. Supersonic land-speed-record vehicle ground-flow interactions studied using thermochromic liquid crystals and computational fluid dynamics. Published as Paper EXP-19 at the 13th International Heat Transfer Conference, Sydney, Australia, August 13-18, 2006.

Experimental methods for validation of computational fluid dynamics codes. D. Aeschliman and W. Oberkampf. AIAA J., 1998, 36(5), 733-741.

Aerofoil RAE 2822 - Pressure distributions, and boundary layer and wake measurements. Cook, P., M. A. McDonald, and M. C. P. Firmin. Software evaluation database based on experimental data. The 1979 AGARD Report AR 138.

Krige, D. A statistical method for solving certain elementary issues in valuing Witwatersrand mines. Journal of the Chemical, Metallurgical, and Mining Society of South Africa, Volume 52, Issues 119–138 (1951).

La thorie des variables rgionalises et ses applications. Matheron, G., 1970. (Les Cahiers du Centre de Morphologie Mathmatique de Fontainebleau, Ecole Suprieure des Mines de Paris, Paris).

Response surface construction for aerodynamic functions using kriging and cokriging. Laurenceau, J., and Sagaut, P. AIAA J., 2008, 46(2), 498-507.